Research Square

Preprints are preliminary reports that have not undergone peer review.
They should not be considered conclusive, used to inform clinical practice,
or referenced by the media as validated information.

A Convolution-Based Thermal Digital Twin for WAAM with Parameter Calibration and Process Temperature Correction

Yann Ledoux

yann.ledoux@grenoble-inp.fr

University Grenoble Alpes, CNRS, Grenoble INP, G-SCOP

Nicolas Beraud

University Grenoble Alpes, CNRS, Grenoble INP, G-SCOP

Research Article

Keywords: Wire arc additive manufacturing, thermal modelling, digital twin, Gaussian convolution, parameter calibration, thermocouple measurements.

Posted Date: November 17th, 2026

DOI: https://doi.org/10.21203/rs.3.rs-11353029/v1

License: This work is licensed under a Creative Commons Attribution 4.0 International License.
Read Full License

Additional Declarations: No competing interests reported.

A Convolution-Based Thermal Digital Twin for WAAM with Parameter Calibration and Process Temperature Correction

Yann Ledoux[a*], Nicolas Beraud[a]

University Grenoble Alpes, CNRS, Grenoble INP, G-SCOP, 38000 Grenoble, France
Corresponding author: yann.ledoux@grenoble-inp.fr

Abstract

Wire arc additive manufacturing (WAAM) enables the production of large metallic components at high deposition rates, but its thermal history remains challenging to predict efficiently. This study presents a voxel-based thermal model as part of a WAAM digital twin, in which heat diffusion is computed using Gaussian convolution. The model is used to investigate uncertain thermal parameters, predict process indicators and update the simulated thermal state using recorded thermocouple measurements. A one-at-a-time sensitivity analysis was conducted, and the energetic efficiency and convective heat-transfer coefficient were calibrated using experimental temperature histories from a zigzag deposition case. The calibrated model was then assessed for a raster strategy. Joint calibration reduced the reported global mean absolute deviation (MAD) from 20.44 °C to 17.32 °C for the zigzag case. For the raster strategy, the simulation agreed with the experimental measurements, with a MAD of 20.90 °C and a Pearson coefficient of 0.947. Simulations showed that welding-source power and torch travel speed strongly affected the model-predicted melt-pool volume. Finally, recorded thermocouple data were used offline to impose a temperature field in the instrumented region. This measurement-informed update provides a basis for further development of a thermal digital twin for WAAM, but does not constitute real-time synchronization or closed-loop control.

Keywords
Wire arc additive manufacturing; thermal modelling; digital twin; Gaussian convolution; parameter calibration; thermocouple measurements.

Acknowledgements
The authors are grateful to S.mart Grenoble Alpes for their technical support.

Author contributions
Yann Ledoux: Conceptualization, Methodology, Data curation, Validation, Writing – original draft.
Nicolas Béraud: Conceptualization, Methodology, Data curation, Visualization, Validation, Writing – review and editing.
All authors read and approved the final manuscript.

Funding
This research received no external funding.

Conflict of interest
The authors have no conflict of interest to declare that are relevant to the content of this article.

Data availability
The data supporting the findings of this study are available from the authors upon request.

Ethics, Consent to Participate, and Consent to Publish declarations: not applicable.

1 Introduction

Wire Arc Additive Manufacturing is a metal additive manufacturing process based on the deposition of successive weld beads generated from a continuously fed wire and an electric arc. Compared with other metal additive manufacturing technologies, WAAM offers high deposition rates and is particularly suitable for the production of large-scale metallic components. Pattanayak and Sahoo, in [1], reviewed the main process configurations and industrial opportunities associated with gas metal arc welding based additive manufacturing.

Despite these advantages, the industrial deployment of WAAM remains limited by difficulties in controlling the geometry, thermal history and mechanical properties of manufactured parts. At the material and the process scales, WAAM may lead to porosity, deformation, oxidation, cracking, residual stresses or delamination. Wu et al. [2] showed that these defects are strongly related to the process conditions and to the thermal history experienced by the deposited material. Béraud et al., in [3], demonstrated the relevance of thermal simulation for analyzing a porosity-related indicator based on melt-pool volume in aluminum WAAM.

For the part scale, this thermal history directly influences the geometry of the deposited beads and the dimensional accuracy of the manufactured part. [4] investigated the influence of the temperature and substrate geometry for aluminum alloy weld beads. The thermal history also affects the residual stress state. [5] showed that inter-layer dwell time influences the stress field in thin-walled WAAM parts.

Several process parameters influence the thermal state and its history all along the part production. These include the welding power, torch travel speed, wire-feed speed, initial temperature of the manufacturing plate and inter-layer dwell time. The dwell time determines the duration available for cooling before deposition of the following layer. Li and Xiong [5] showed that this parameter can significantly affect the stress field in thin-walled WAAM components. The heat input also influences the microstructure and mechanical properties of aluminum alloys deposited by WAAM, as reported by [6]. Temperature and substrate conditions can additionally affect the geometry of individual deposited beads, as shown by [4].

To manage such an operation, numerical simulation is widely used to investigate these phenomena and to support the selection of process parameters. Finite element models can represent the movement of the heat source, material deposition, complex geometries and temperature-dependent material properties. Montevecchi et al. [7] developed a finite element model for the WAAM process. [8] considered three-dimensional finite element analysis with clamping conditions. Gokhale and Kala [9] investigated the thermal behavior of a TIG-WAAM process using finite element analysis. Even if these models lead to a good accuracy, these conventional high-fidelity simulations require substantial computation time. During process development, several manufacturing strategies may need to be compared by varying the torch trajectory, welding parameters, deposition rate, initial substrate temperature or inter-layer dwell time. A large number of simulations may therefore be required. This point has been highlighted by [10] where the authors have identified computational efficiency as one of the major challenges in modeling WAAM processes.

The development of a fast and versatile simulation model is therefore essential for establishing a practical link between virtual simulation and physical production.

Several approaches have been proposed to reduce computation time. [11] investigated methods for large-scale simulation of residual stress and distortion in WAAM. Moreira et al. [12] proposed an adaptive finite element framework for part-scale thermal analysis in additive manufacturing. Explicit time-integration schemes have also been investigated as a means of accelerating thermal simulations, as reported by [13]. Another approach based on data-driven models is also explored in the literature. Farias et al. [14] used artificial neural networks to predict the interpass temperature of a WAAM wall from

finite element simulation results. Zani et al. [15] proposed a WAAM metamodel based on basis spline entities. These approaches can provide rapid predictions after an offline training or fitting phase. Their applicability may nevertheless depend on the available training database, the considered geometry and the range of process conditions represented in the data.

Another kind of approach to obtain fast thermal simulations of WAAM process is based on voxel representation of the geometrical space and a convolution calculation of heat diffusion. [16] showed that such a method could reproduce the main characteristics of experimentally measured temperature histories while significantly reducing computation time compared with a finite element reference model.

The use of a fast model is also relevant to the development of a digital twin. A digital twin is not limited to an independent numerical simulation. It provides a virtual representation of a physical system and establishes a connection between the virtual and physical domains through data exchange, state estimation and prediction. In additive manufacturing, this connection is particularly important because the thermal state of the substrate or manufacturing plate may vary from one deposition to another. An incorrectly estimated initial temperature can propagate through the simulation and generate errors in the predicted temperature field, melt-pool behavior and subsequent thermal history.

The reliability of a thermo-physical digital twin therefore depends not only on the formulation of its physical model, but also on its ability to account for uncertain parameters and variations in the manufacturing conditions. In the present study, the emissivity ε, the convective heat transfer coefficient h, the energetic efficiency η, and the thermal diffusivity α are considered uncertain or imperfectly known quantities. These parameters are related to the representation of radiative and convective heat exchange and to the initial thermal state. Their influence on the simulation results is investigated using the available experimental information.

Parameter identification is not considered as an objective in itself. It is treated as a necessary step for developing a thermo-physical digital twin that is computationally efficient, sufficiently reliable and suitable for process-oriented decision support. The aim is not only to obtain a set of calibrated parameters, but also to evaluate the sensitivity of the fast simulation and determine whether its predictions are sufficiently reliable for supporting manufacturing decisions.

Once identified, the digital twin can be used to study the influence of several process variables on the thermal behavior of the deposition. In this work, the analysis focuses on the initial temperature of the manufacturing plate, the welding power and the travel speed of the welding torch. These variables represent the main sources of process variability as discussed in the work of [17].

The response of the digital twin is evaluated using indicators related to the melt pool and the thermal state of the deposited material. The indicators considered in this study are the melt-pool volume, the mean deposition-surface temperature and, for the measurement-informed comparison, the temperature at the next deposition. [3] showed the relevance of melt-pool volume as an indicator for analyzing porosity-related behavior in aluminum WAAM. In the present work, these indicators are considered both as measures of the agreement between the physical process and its virtual representation and as potential criteria for process adjustment.

The research question addressed in this study is therefore:

How can a fast thermo-physical digital twin, supported by parameter identification and incorporating the initial thermal state, predict melt-pool behavior and support the selection of WAAM process parameters?

To answer this question, the study first quantifies the effect of an incorrectly estimated initial temperature on the simulation results. The uncertain physical parameters are then identified using the available experimental information, and the predictive capability of the fast digital twin is evaluated.

Finally, virtual experiments are conducted to analyze the effects of the initial temperature of the manufacturing plate, the welding power and the travel speed of the welding torch.

The main contributions of this study are:

1. the sensitivity analysis and identification of uncertain thermal parameters;
2. the evaluation of the predictive capability of the calibrated digital twin;
3. the analysis of the effects of the initial plate temperature, welding power and travel speed of the torch;
4. the use of melt-pool volume and temperature indicators to support process-oriented decision-making;
5. the definition of a framework for rapidly comparing process settings while maintaining a target thermal state.

The identification procedure is therefore positioned as the link between physical measurements, virtual simulation and rapid process-oriented decision-making. The proposed framework does not yet include adaptive or closed-loop control of the manufacturing system. Such a control strategy constitutes a perspective that could use the calibrated digital twin to adjust process parameters during fabrication.

2 Thermal digital twin architecture

The proposed digital twin is designed to connect the physical WAAM process with a fast thermo-physical model. The main objective is to represent the thermal state of the manufacturing process integrating data from the real process aiming at providing rapid predictions to support process analysis and parameter selection. For that, a connection is defined between a physical manufacturing system and its digital representation through data exchange and synchronization phases.

[18] proposed an implementation architecture for WAAM digital twins based on ISO 23247, emphasizing connectivity, interoperability and real-time decision support. A recent review by [19] also identified monitoring, modeling, optimization and process control as central functions of digital twins in additive manufacturing. The works of [20] similarly highlight the importance to combine physical modeling, process monitoring, prediction and data management in WAAM digital twin model.

The architecture considered in this work is composed of five main components: the physical WAAM system, the data-acquisition system, the virtual thermo-physical model, the parameter identification module and the decision-support layer.

The physical system includes all the elements defining the real process like the welding source, torch, wire, robot or positioning system, manufacturing plate, deposited part and support. During welding operation, as material is deposited and heat is introduced into the manufacturing domain, this leads to updated the different states of their values. The main process variables include the welding current, welding voltage, torch position, travel speed, wire-feed speed, arc status, deposited geometry and initial temperature of the manufacturing plate.

The data-acquisition system provides information to describe the actual manufacturing operation. Particularly, process data are obtained from the welding source and robot controller, while temperature measurements are acquired using sensors positioned on the surface of the manufacturing plate. These measurements provide indirect information about heat accumulation in the substrate and heat transfer through the plate. They do not directly measure the melt-pool temperature, but they are used to evaluate the consistency between the physical and virtual thermal states.

Local monitoring techniques can provide additional information about thermal evolution, melt-pool geometry near the deposition zone. For example, optical and near-infrared measurements can be used to detect thermal deviations during aluminum WAAM deposition [21]. In such a case, the integration

of local measurements into a digital twin requires sensor calibrations, temporal synchronization, signal processing and rapid interpretation of the data. In the present study, thermocouples on the manufacturing plate are used to bring thermal observations, whereas the melt-pool indicators are calculated from the virtual model.

The virtual model represents the manufacturing domain using a voxel-based description. It calculates material deposition, energy input, heat losses and heat diffusion during the process. The model can use nominal or measured process parameters and can incorporate the initial thermal state of the manufacturing plate. The model definition is presented in the section 3.

The parameter-identification module uses the available experimental information to estimate uncertain parameters, including the diffusivity, the convective heat-transfer coefficient, the energetic efficiency and the initial temperature. The identified parameters are used to improve the accuracy of the virtual model. The calibration and validation procedures are presented in Section 4.

The last component corresponds to the decision-support layer. It uses the predicted melt-pool and thermal state to adapt the process configurations and identify parameter combinations leading to manage the thermal state. The initial temperature of the manufacturing plate, the welding power and the travel speed of the welding torch are varied in virtual experiments. Automatic modification of these variables during fabrication is not implemented and remains a perspective for future adaptive or closed-loop control. The information flow of the proposed architecture is illustrated in figure 1.

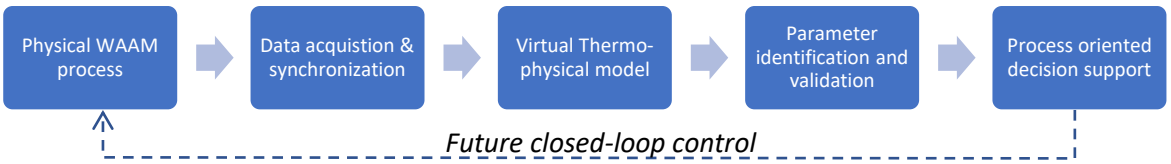


Figure 1 : proposed thermal digital twin architecture for WAAM process

3 Fast convolution thermo-physical model

3.1 Voxel representation

The manufacturing domain is discretized into cubic voxels of size d. The volume a one voxel corresponds to V= d^3. At time t, the material state is represented by the matrix:

$$M(t) = [m_{xyz}(t)] \quad (1)$$

where:

$$m_{xyz}(t) = \begin{cases} 1, & if\ voxel\ (x,y,z)\ contains\ material, \\ 0, & otherwise. \end{cases} \quad (2)$$

The thermal state is represented by the energy matrix composed of the energy state of each voxel $e_{xyz}(t)$:

$$E(t) = [e_{xyz}(t)] \quad (3)$$

The energy of an empty voxel is set to zero. For a material-filled voxel, the temperature is calculated from the stored energy:

$$T(t) = \frac{E(t)}{\rho . c . V} \quad (4)$$

The voxel formulation follows the fast WAAM simulation approach proposed by [16]. Its main advantage is that the same numerical structure can be used for different part geometries without constructing a new unstructured finite element model for each case.

3.2 Initial state and material deposition

At the beginning of the simulation, the material field is initialized from the manufacturing plate geometry. Voxels belonging to the plate are activated and assigned the initial temperature *Tini*.

During a time step, newly deposited material is described by the matrix ΔM(t). The material field is updated according to:

$$M(t + \Delta t) = M(t) + \Delta M(t) \tag{5}$$

This formulation assumes that each voxel is either empty or filled. A finer description of the bead geometry could be obtained by reducing the voxel size or by introducing fractional filling values.

3.3 Welding energy input

The useful welding energy introduced during one time step is calculated from the welding voltage, welding current and energetic efficiency:

$$Q(t) = \eta . U(t) . I(t) . \Delta t \tag{6}$$

The energy is divided into a contribution associated with the newly deposited material and a contribution transferred to the existing material:

$$Q(t) = Q_{wire}(t) + Q_{sub}(t) \tag{7}$$

In the present formulation:

$$Q_{wire}(t) = Q_{sub}(t) = \frac{1}{2} Q(t) \tag{8}$$

The energy associated with the deposited voxels is distributed as:

$$\Delta e_{wire,xyz}(t) = \frac{Q_{wire}(t)}{N(t)} \Delta m_{xyz}(t) \tag{9}$$

where N(t) is the number of voxels activated during the time step.

The energy transferred to the existing material is distributed using a double-ellipsoidal heat source. [22] introduced this type of heat-source representation for welding simulation. In the present formulation:

$$\Delta e_{sub,xyz}(t) = \int_{V_{xyz}} q(x, y, z, t)\, dV \tag{10}$$

where $q(x, y, z)$ is the local energy density.

The heat-source parameters are selected so that:

$$\sum_{x,y,z} \Delta e_{sub\ xyz}(t) = Q_{sub}(t) \tag{11}$$

The energy field after welding input is:

$$E_w(t) = E(t) + \Delta E_{wire}(t) + \Delta E_{sub}(t) \tag{12}$$

3.4 Convection, radiation and exchange

The temperature after the welding-energy input is calculated as:

$$T_w(t) = \frac{E_w(t)}{\rho . c . V} \tag{13}$$

Convective heat exchange is calculated using:

$$\Delta E_{conv} = h . \Delta t . S(t) \odot (T_w(t) - T_{amb}) \tag{14}$$

where h is the convective heat-transfer coefficient and $S(t)$ is the matrix of exposed surfaces.

Radiative exchange is calculated according to:

$$\Delta E_{rad} = \sigma_B . \varepsilon . \Delta t . S(T) \odot \left(T_w(t)^{\odot 4} - {T_{amb}}^4\right) \tag{15}$$

where ε is the emissivity and σ_B is the Stefan-Boltzmann constant.

The energy field before heat diffusion is therefore:

$$E_{exch}(t) = E_w(t) - \Delta E_{conv}(t) - \Delta E_{rad}(t) \tag{16}$$

3.5 Heat diffusion by Gaussian convolution

The heat-diffusion calculation is based on the analytical solution of the heat equation. [23] established the representation of heat diffusion using a Gaussian heat kernel.

The thermal diffusivity is:

$$\alpha_l = \lambda_l / (\rho_l c_l) \tag{17}$$

The standard deviation of the Gaussian kernel is:

$$\sigma = \sqrt{2\alpha\Delta t} \tag{18}$$

The heat-diffusion field is calculated by:

$$E_{cond}(t) = E_{exch}(t) \otimes k_e \tag{19}$$

where k_e is the discrete heat kernel.

The kernel is normalized according to:

$$\sum_{x,y,z} k_e(x,y,z) \; = \; 1 \tag{20}$$

This normalization ensures energy conservation for the diffusion operation on an infinite domain. Because the manufacturing domain is finite, the convolution is corrected to prevent energy from being transferred irreversibly into empty voxels:

$$E_{cond}(t) = E_{exch}(t) \otimes k_e + (\mathbf{1} - M(t+\Delta t) \otimes k_e) \odot E_{exch}(t) \tag{21}$$

The correction returns to the material domain the energy that would otherwise cross the material boundary. The total energy is conserved during the diffusion step, while the global energy balance can still change because of welding input, convection and radiation.

3.6 Model assumptions

The model uses several simplifying assumptions to preserve computational efficiency:

- the domain is represented by cubic voxels;
- the material is considered homogeneous and temperature independent;
- representative thermal properties are used during heat diffusion;
- radiation is calculated without detailed view factors;
- the bead geometry is limited by the voxel resolution;
- energy exchanges and diffusion are treated as separate operations.

The validity of these assumptions depends on the intended use. The model is designed for rapid process evaluation and thermal-state estimation rather than for replacing high-fidelity finite element simulations in all applications.

4 Experimental setup and methodology

The experimental study considers the fabrication of an aluminum alloy (Al5356) thin wall using a WAAM cell. The experimental configuration is based on the reference case described by [24], which provides both experimental temperature data and finite element simulation results.

The system includes a robotic positioning device (Yaskawa MA1440 six-axis robot), a welding source (Fronius T.P.S CMT 4000), a wire-feed system, a manufacturing plate (250 x 250 x 5 mm) and a support arrangement. The plate is positioned on a firebrick to ensure no conduction with other parts, leading to only convection and radiation losses. The deposited wall is manufactured layer by layer according to a predefined torch trajectory. The welding parameters are available in Table 1. A typical experimental setup is defined to measure during the welding operation the thermal evolution of the manufacturing plate. The positions of the six thermocouples (P1 to P6) are available in Figure 2.

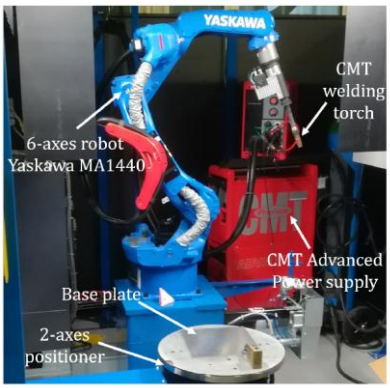


Figure 2 : Experimental WAAM system

Parameters	Welding-source power (U.I)	Travel speed	Idle time	Acquisition duration	WFS synergic	EP/EN	Synergy law
Units	W	mm/s	s	s	(m/min)		CMT advanced
Values	960	10	2	170	5	+1	1368

Table 1: Manufacturing parameters

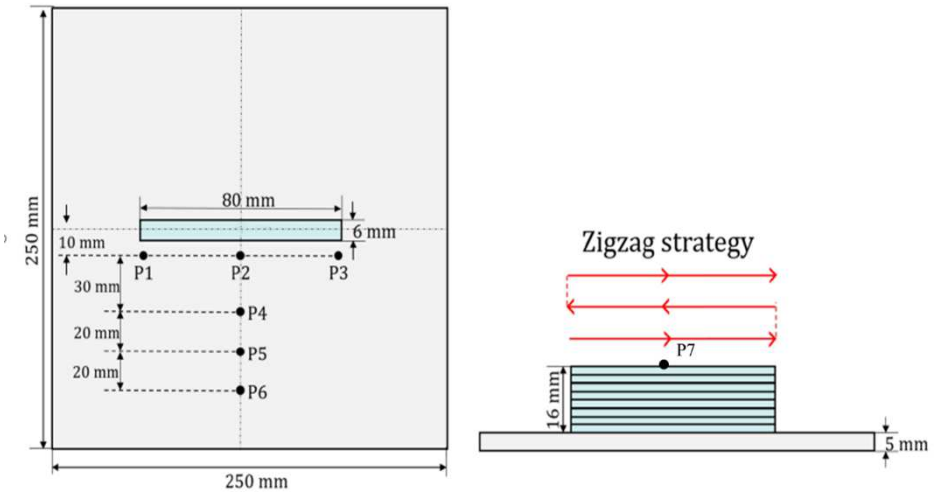


Figure 3: Experimental design (Chergui et al., 2021)

5 Sensitivity analysis, parameter identification and validation

Based on the thermal simulation, it is proposed to perform a sensitivity analysis (one at a time approach). The experimental case related to zigzag strategy was used to perform the sensitivity analysis and calibrate the model parameters. The main goal is to identify the most relevant parameters influencing the operation. The studied parameters were related to the energetic efficiency η, the convective heat-transfer coefficient h, the emissivity ε and the thermal diffusivity α around their nominal values. These coefficients correspond to parameters whom the effective value was hard to precisely defined. The data are available in Table 2.

The model response was evaluated using the global mean absolute error between the simulated and experimental temperature histories obtained in experimental tests.

Symbol	Ref. value	Tested Range
η	0,83	From 0,75 to 0,95
h	20 Wm−2K−1	from 5 to 50$Wm^{-2}K^{-1}$
ε	0,77	From 0,10 to 0,90
α	5.50×10^{-5} $m^2\,s^{-1}$	from 4,85 à $5,50\times10^{-5}$ $m^2\,s^{-1}$

Table 2: Tested ranges for the simulation parameter

The MAD indicator was used to evaluate the influence of parameters on the temperature fields (see equation 22)

$$\mathrm{MAD}=\frac{1}{N}\sum_{j=1}^{N}\left|x_j-\bar{x}\right| \quad (22)$$

Figure 4 plots the different evolution of the MAD according to the parametric sensitivity. The results show that η and h have the strongest influence on the prediction error within the investigated parameter ranges. The sensitivity curve for η exhibits a non-monotonic behavior with a variation of 6.4°C. The minimum error is close to η=0.90. This indicates that the nominal value η=0.83 does not provide the best agreement with the experimental data. The convective coefficient also presents a non-monotonic

response, with a minimum in the range of approximately 15 to 18 $W\,m^{-2}K^{-1}$. The later parameter corresponds to the most influential parameter on the studied range leading to a variation of 13°C.
The influence of the diffusivity (α) is weaker, although the curve exhibits a shallow minimum at an intermediate value (influence around 1°C on the MAD). The thermal diffusivity has a very limited effect on the global error over the investigated range. These results suggest that η and h should be prioritized during parameter identification, whereas ε and α can initially be fixed at reference values.

The simultaneous calibration of η and h changed their values from 0.83 to 0.9 and from 20 to 17.86 $W\,m^{-2}K^{-1}$ respectively. The global MAD decreased from 20.44 °C to 17.32 °C, corresponding to an absolute reduction of 3.12 °C and a relative reduction of approximately 15.26%. This improvement indicates a better agreement between the simulated and measured temperature histories. However, because both parameters affect the global thermal balance, their individual identifiability should be assessed using independent validation data.

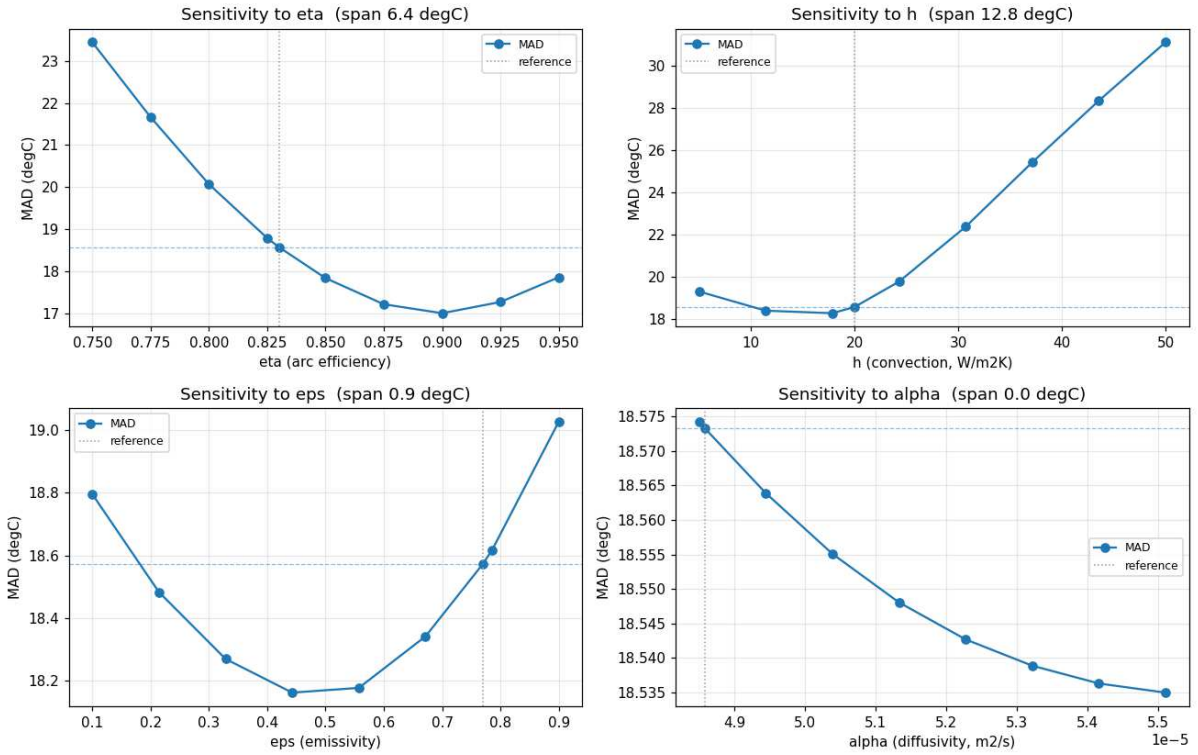


Figure 4: Sensitivity analysis of the parameters on the simulation

The experimental results reported by [24] are compared with the temperatures simulated for the zigzag deposition strategy. Figure 5 shows the temperature evolution at each thermocouple location. The simulated curves reproduce the main trends observed experimentally, including the successive temperature peaks associated with the torch passes and the subsequent cooling phase. The responses at P1 to P3 show more pronounced fluctuations, while those at P4 to P6 are smoother, consistent with their locations relative to the deposited wall. Some differences remain in the amplitude and timing of individual peaks. The MAD is equal to 17.32°C and the Pearson coefficient is equal to 0.969.

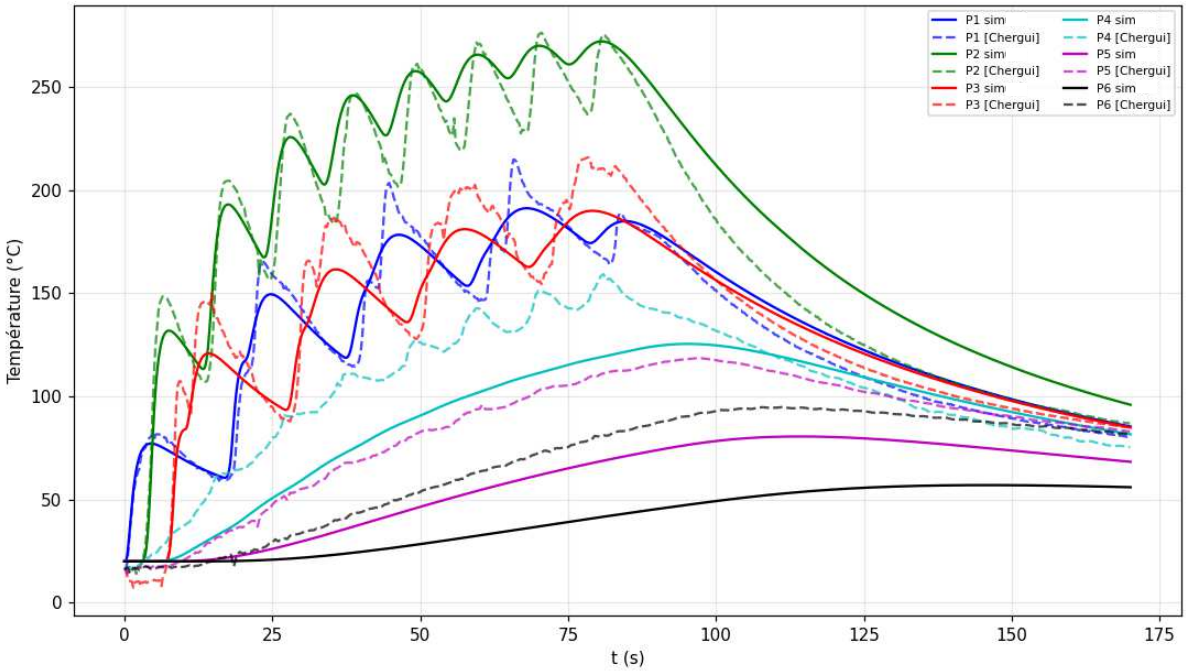


Figure 5: Simulation of the built part assuming zigzag strategy

5.1 Validation on raster strategies

To evaluate the calibrated model on a different deposition strategy, the raster case was simulated using the values of η and h identified from the zigzag case, without further parameter adjustment. The raster case was therefore used to evaluate the calibrated model on a different deposition strategy assuming same process configuration (listed in Table 1).

For this raster deposition strategy, Figure 6 compares the simulated temperature histories with the experimental measurements reported by [24]. The model reproduces the overall heating and cooling trends across the sensor locations, including the successive temperature increases during deposition and the subsequent cooling phase. The experimental curves show sharper fluctuations than the simulated curves, particularly at P1 to P3, while the responses at the more distant locations are smoother. For P1 to P6, excluding P4 (experimental results not available), the reported mean absolute deviation is 20.90 °C, and the Pearson correlation coefficient is 0.947. These results indicate good agreement in the overall temporal evolution, although differences remain in the amplitude and timing of individual temperature peaks.

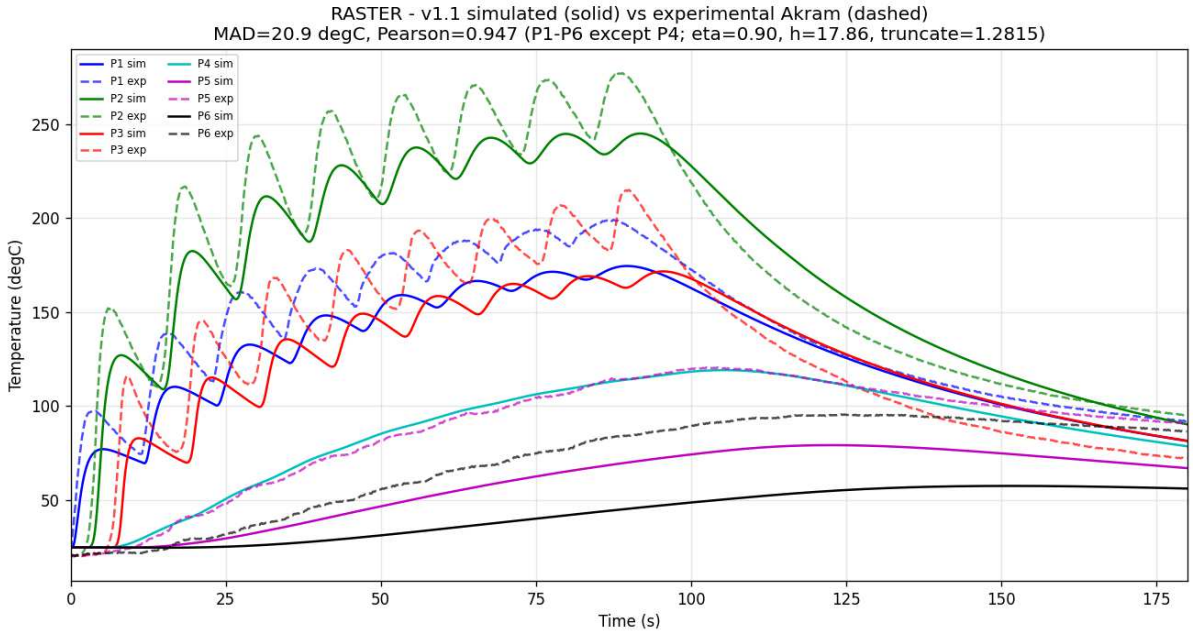


Figure 6: Simulation of the built part assuming raster strategy

5.2 Computational performance

For a process duration of 170 s, the convolution-based simulation required 150 s of computation on a computer equipped with an Intel Core i7-8700 CPU running at 3.20 GHz. As a comparison, the same FEM simulation as that reported by [24] required 12,000 s for the same process duration. The convolution-based model therefore reduced the computation time by a factor of 80 relative to the FEM reference. Both simulations are run the same computer. Its real-time factor, defined as the process duration divided by the simulation runtime, was 1.13 (170/150), meaning that the 170 s process was simulated in 150 s.

6 Virtual process analysis

A one-at-a-time sensitivity analysis was conducted around the initial configuration, assuming an initial substrate temperature of 20 °C, an welding source power input of 960 W, and a torch travel speed of 10 mm s^{-1}. In each simulation, one parameter was varied while the others were kept at their initial values. The calibrated thermal parameters, including η=0.90 and h=17.86 $Wm^{-2}K^{-1}$, were constant. The outputs considered were the mean melt-pool volume, defined as the volume of voxels above 650°C, and the mean deposition-surface temperature.

The welding source power input was varied from 883 to 1036 W, corresponding to a range of approximately ±8% around the initial value according to the conclusion of [25]. Increasing welding source power generally increased the predicted melt-pool volume, particularly in later layers as heat accumulated. Compare to the results obtained with the initial values, the mean melt-pool volume varied from −47% to +55%, while the mean deposition-surface temperature ranged from −7% to +7%. The threshold-based melt-pool volume was therefore more sensitive to welding source power than the mean deposition-surface temperature.

The initial substrate temperature was varied from 20 to 50 °C. This range represents possible substrate warming over the production day as heat accumulates between successive manufacturing operations. It is treated here as a sensitivity scenario. The deposition-surface temperature histories remained close: the mean temperature changed by approximately 0 to +1%, while the mean melt-pool volume increased by up to approximately +9%. This difference reflects the threshold-based volume definition, under which a modest temperature change may cause voxels to cross the 650 °C threshold.

Torch travel speed was varied from 9 to 11 mm s−1, or ±10% around the initial value. This interval was selected to examine the effect of variation in the average robot-controlled torch speed. At constant welding source power, lower travel speed increases the energy input per unit length, whereas higher

speed reduces it. The mean melt-pool volume varied by approximately −51% to +75%, while the mean deposition-surface temperature varied by approximately −7% to +10%.

Overall, welding source power and travel speed had the strongest effects on the predicted melt-pool volume. The initial substrate temperature had a smaller, but still detectable, influence. Since the parameters were varied independently, these results do not capture interactions between them or identify an optimal parameter combination. The melt-pool volume should also be interpreted as a model-based indicator defined by the 650 °C threshold, rather than as a direct measurement of the physical liquid pool.

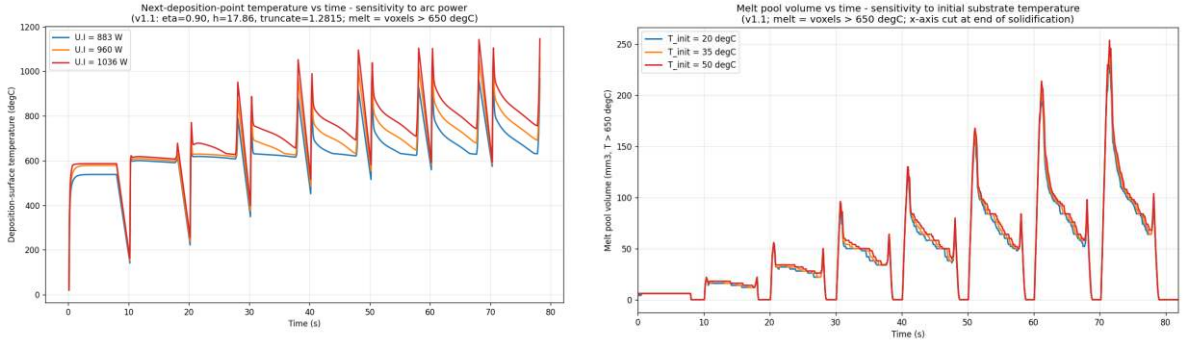


Figure 7: Influence of the power on the temperature fields and the melt-pool volume

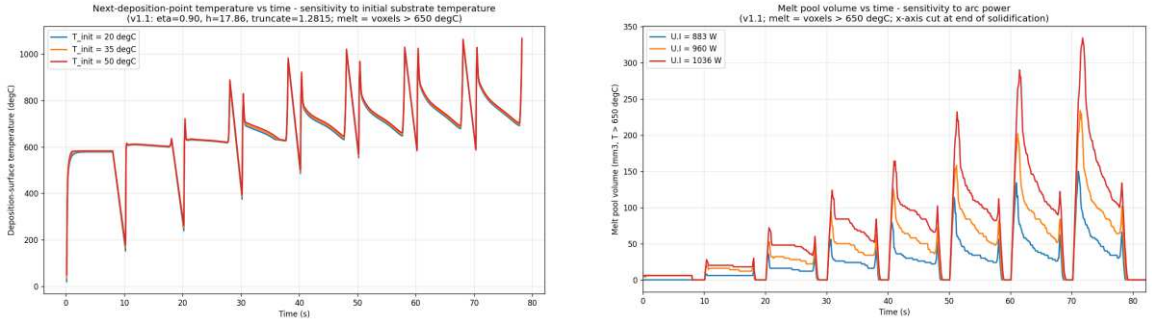


Figure 8: Influence of the initial plate temperature on the temperature fields and the melt-pool volume

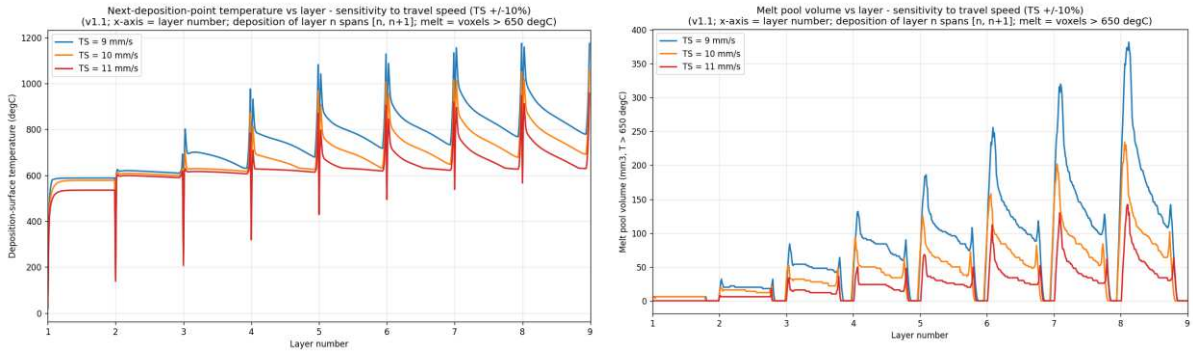


Figure 9: Influence of the torch speed on the temperature fields and the melt-pool volume

7 Interaction between in-situ measurement and simulation

To investigate the integration of in-situ measurements into the thermal model, a measurement-informed simulation was compared with a baseline simulation in which the substrate temperature field was fully simulated. An illustration of the simulation model is available in Figure 10. Although the temperatures were measured in situ during the WAAM operation, they were not streamed to the model during the

process. In the present example, the recorded thermocouple time series were used offline and interpolated onto the simulation grid.

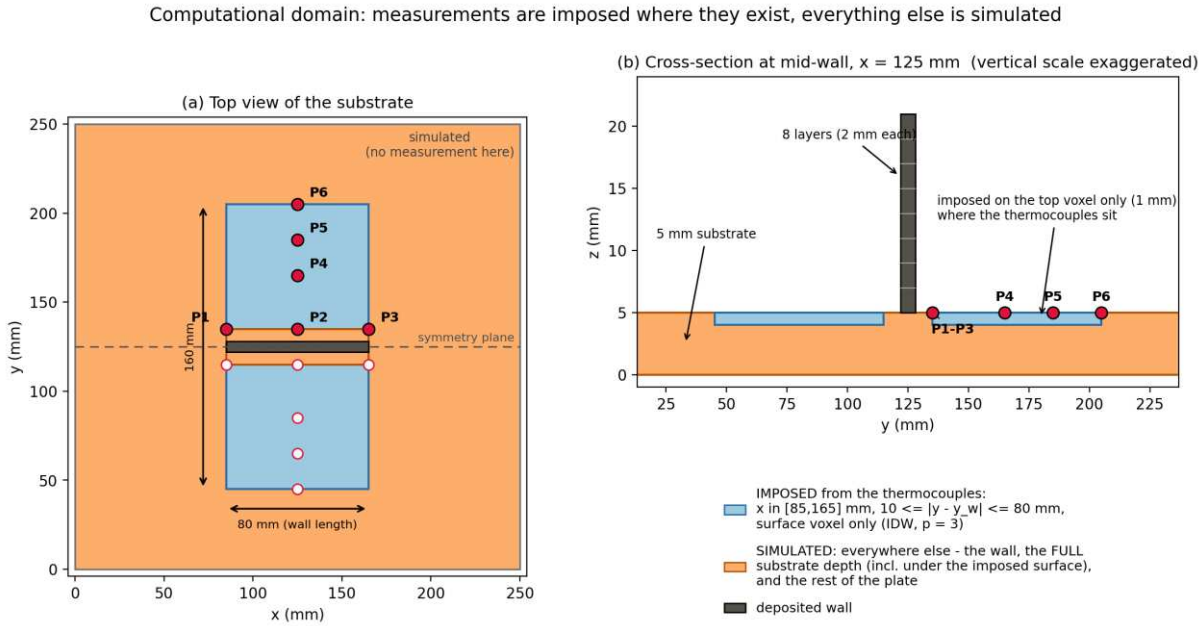


Figure 10: Main simulation characteristics

The six thermocouple time series were linearly interpolated onto the simulation time grid. At each time step, a spatial temperature field was reconstructed from the six sensor readings and their six mirrored locations, obtained by reflecting the sensors about the wall's symmetry plane. Inverse-distance weighting was used:

$$T(x,t)=\frac{\sum_{i=1}^{12} w_i T_i(t)}{\sum_{i=1}^{12} w_i},\ w_i = d_i^{-p},\ p=3 \tag{23}$$

where d_i is the in-plane Euclidean distance between the point x and sensor i, or its mirrored location. The normalized spatial weights were calculated once because the sensor and part geometry remained fixed. Thus, the reconstruction at each time step required only a weighted sum of the sensor temperatures.

The reconstructed field was imposed in the measurement-informed region and applied uniformly through the substrate thickness. Outside this region, the temperature field remained simulated. At the initial time, the reconstructed field was used within the measurement-informed region, while the rest of the substrate was initialized using the mean temperature measured at t=0. This procedure incorporates the measured thermal evolution into the simulation while retaining the model's prediction in regions without measurements.

The reconstructed temperature maps at times 50s is shown as an illustration in Figure 11. They illustrate how the discrete thermocouple readings are used to estimate the spatial thermal field. Figure 12 compares the resulting melt-pool volume and next-deposition temperature with those predicted by the fully simulated part. The curves largely overlap, indicating that incorporating the measurement-informed field has a limited effect on these two indicators for the case considered. The approach therefore provides a means of synchronizing part of the virtual thermal state with in-situ recorded measurements, while simulation continues in regions not covered by the measurement update. It does not, however, implement automatic adjustment of the physical process parameters or closed-loop process control.

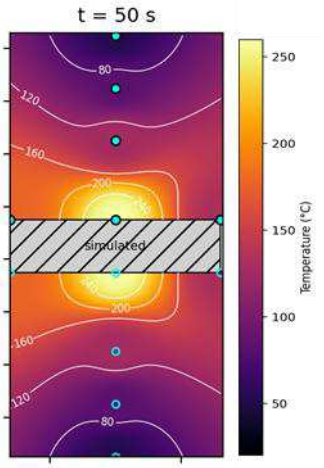


Figure 11: Illustration of the imposed thermal field at 50s

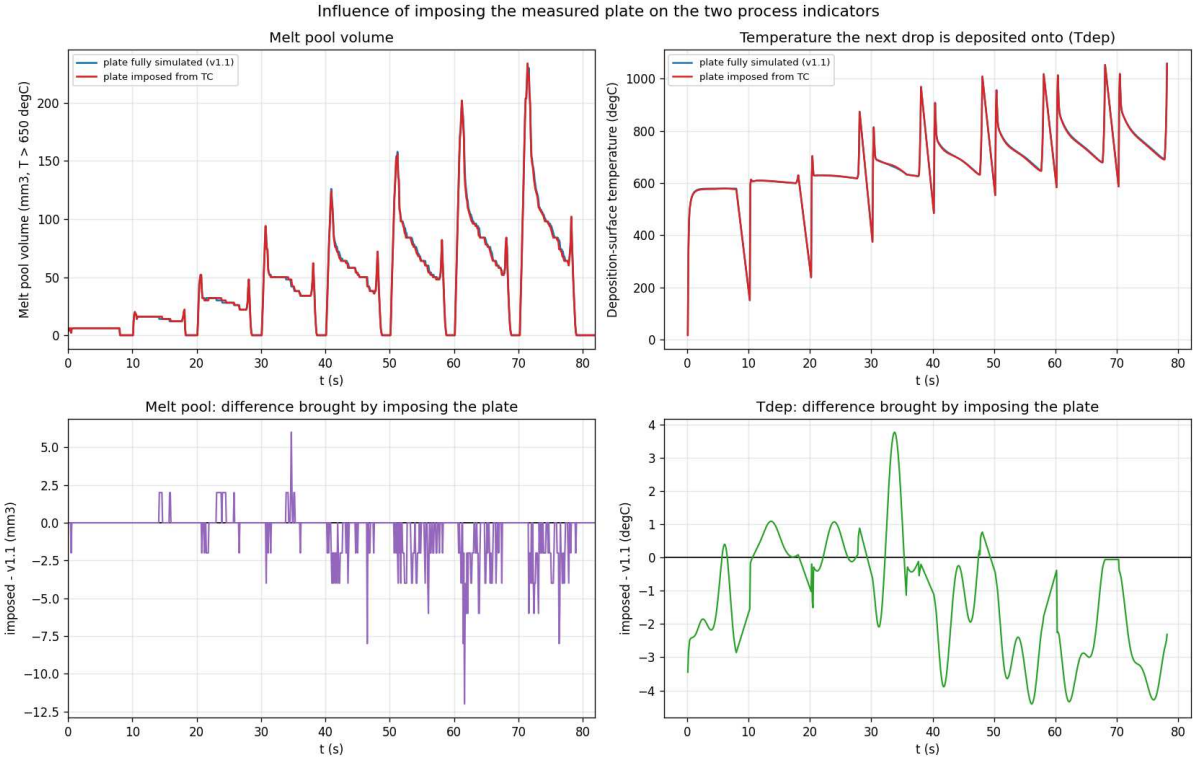


Figure 12: numerical results assuming the thermal measurements on built plate

8 Discussion

The results demonstrate the potential of the convolution-based model for rapid thermal analysis of WAAM. Comparisons with experimental temperature histories for the zigzag and raster deposition strategies show that the model captures the main heating and cooling trends. However, the simulated curves are smoother than the measured signals and do not reproduce all local temperature peaks. This is consistent with the model's reduced spatial resolution, simplified heat-source representation and thermal boundary assumptions.

Calibration of the energetic efficiency and convective heat-transfer coefficient improved agreement with the experimental data. The calibrated values changed from η=0.83 to 0.90 and from h=20 to 17.86 $W\,m^{-2}K^{-1}$, while the reported temperature error decreased from 20.44 °C to 17.32°C. These parameters influence the global thermal balance in opposing ways: increasing η raises the energy input,

whereas reducing h decreases convective losses. Their combined identification should therefore be interpreted with care, as the available measurements may not fully distinguish their individual effects.
The one-at-a-time sensitivity analysis indicates that welding source power and torch travel speed have the strongest influence on the predicted melt-pool volume. Changes in the initial substrate temperature from 20 to 50 °C, have a smaller effect on the mean deposition temperature, although a detectable change in volume remains.
The measurement-informed simulation incorporates temperatures reconstructed from six thermocouples using inverse-distance weighting and symmetry about the wall. For the case studied, its melt-pool-volume and next-deposition-temperature predictions remain close to those from the fully simulated baseline. Thus, imposing the reconstructed field provides a means of updating the virtual thermal state. The reconstructed field remains dependent on sensor placement, the interpolation method and the assumed spatial distribution of temperature. This later point is a critical advantage compare to classical finite element simulation where the introduction of external temperature point needs computation effort to evaluate a thermal equilibrium and may introduce important discontinuities in the numerical simulation.
More to that, incorporating measured process data, particularly time-resolved welding source power and torch speed, could help represent actual process variations that are not captured by nominal settings. Temperature measurements may also help compensate for residual discrepancies arising from calibration and model assumptions. The computational benefit of imposing measured temperatures will depend on whether this reduces the domain requiring numerical solution. This benefit should be quantified through runtime comparisons. Since measurements are used to construct the imposed field, independent sensors or experiments would be needed to assess predictive improvement without data reuse.

9 Conclusion

This study presents a fast convolution-based thermal modelling framework for WAAM that combines uncertain-parameter calibration, process sensitivity analysis and a thermocouple-informed update of the virtual thermal state. Comparisons with experimental temperature histories for the zigzag and raster cases show that the model captures the main heating and cooling trends, although local temperature peaks are not reproduced in full. The sensitivity analysis further indicates that welding source power input and torch travel speed are important factors affecting the model-predicted, threshold-based melt-pool volume.
A key step toward a thermal digital twin is the interaction between the physical process and its virtual representation. In the present approach, recorded thermocouple measurements are replayed offline and aligned with the simulation time grid to reconstruct and impose a temperature field in the instrumented region. This allows the virtual thermal state to incorporate information from the ongoing or recorded process rather than relying exclusively on nominal initial conditions and calibrated model parameters. The reconstructed field remains dependent on sensor placement and the interpolation assumptions, and its effect on the two process indicators considered here is limited for the tested case. Nevertheless, this measurement-to-model connection provides a basis for updating the simulation when the actual thermal state differs from the predicted state.
A more complete digital-twin implementation would also use data from the welding source and robot tracking system. Time-resolved welding source power, torch position and actual travel speed could be supplied to the model during deposition, while temperature measurements would update the estimated thermal state. This would allow the virtual representation to follow process variations more closely and could help compensate for residual discrepancies associated with parameter uncertainty and model simplifications. The current study demonstrates measurement-informed thermal-state updating, but not automatic process adjustment or closed-loop control.
Future work should evaluate the approach using independent validation measurements, quantify the computational cost of measurement-informed updates, and integrate synchronized power and torch-tracking data. These developments would support a more complete interaction between the WAAM process, its sensors and the thermal model, and provide a foundation for future predictive or adaptive process control.

10 References

[1] Pattanayak, S., & Sahoo, S. K. (2021). Gas metal arc welding based additive manufacturing: A review. CIRP Journal of Manufacturing Science and Technology, 33, 398-442. https://doi.org/10.1016/j.cirpj.2021.04.010

[2] Wu, B., Pan, Z., Ding, D., Cuiuri, D., Li, H., Xu, J., & Norrish, J. (2018). A review of the wire arc additive manufacturing of metals: Properties, defects and quality improvement. Journal of Manufacturing Processes, 35, 127-139. https://doi.org/10.1016/j.jmapro.2018.08.001

[3] Béraud, N., Chergui, A., Limousin, M., Villeneuve, F., & Vignat, F. (2022). An indicator of porosity through simulation of melt pool volume in aluminum wire arc additive manufacturing. Mechanics & Industry, 23, 1. https://doi.org/10.1051/meca/2021052

[4] Limousin, M., Manokruang, S., Vignat, F., Museau, M., Grandvallet, C., & Béraud, N. (2023). Effect of temperature and substrate geometry on single aluminium weld bead geometry deposited by Wire Arc Additive Manufacturing: Proposition of an experimental procedure. CIRP Journal of Manufacturing Science and Technology, 45, 61-68. https://doi.org/10.1016/j.cirpj.2023.06.010

[5] Li, R., & Xiong, J. (2019). Influence of interlayer dwell time on stress field of thin-walled components in WAAM via numerical simulation and experimental tests. Rapid Prototyping Journal, 25(8), 1433-1441. https://doi.org/10.1108/RPJ-03-2019-0067

[6] Su, C., Chen, X., Gao, C., & Wang, Y. (2019). Effect of heat input on microstructure and mechanical properties of Al-Mg alloys fabricated by WAAM. Applied Surface Science, 486, 431-440. https://doi.org/10.1016/j.apsusc.2019.04.255

[7] Montevecchi, F., Venturini, G., Scippa, A., & Campatelli, G. (2016). Finite element modelling of wire-arc-additive-manufacturing process. Procedia CIRP, 55, 109-114. https://doi.org/10.1016/j.procir.2016.08.024

[8] Wang, X., & Wang, A. (2016). Three-dimensional finite element analysis with clamping in wire and arc additive manufacturing. In 2016 European Modelling Symposium (EMS), 104-108. https://doi.org/10.1109/EMS.2016.028

[9] Gokhale, N. P., & Kala, P. (2021). Thermal analysis of TIG-WAAM based metal deposition process using finite element method. Materials Today: Proceedings, 44, 453-459. https://doi.org/10.1016/j.matpr.2020.09.756

[10] Sampaio, R. F. V., Pragana, J. P. M., Bragança, I. M. F., Silva, C. M. A., Nielsen, C. V., & Martins, P. A. F. (2023). Modelling of wire-arc additive manufacturing: A review. Advances in Industrial and Manufacturing Engineering, 6, 100121. https://doi.org/10.1016/j.aime.2023.100121

[11] Huang, H., Ma, N., Chen, J., Feng, Z., & Murakawa, H. (2020). Toward large-scale simulation of residual stress and distortion in wire and arc additive manufacturing. Additive Manufacturing, 34, 101248. https://doi.org/10.1016/j.addma.2020.101248

[12] Moreira, C. A., Caicedo, M. A., Cervera, M., Chiumenti, M., & Baiges, J. (2022). A multi-criteria h-adaptive finite-element framework for industrial part-scale thermal analysis in additive manufacturing processes. Engineering with Computers, 38(6), 4791-4813. https://doi.org/10.1007/s00366-022-01655-0

[13] Essongue, S., Ledoux, Y., & Ballu, A. (2022). Speeding up mesoscale thermal simulations of powder bed additive manufacturing thanks to the forward Euler time-integration scheme: A critical assessment. Finite Elements in Analysis and Design, 211, 103825. https://doi.org/10.1016/j.finel.2022.103825

[14] Farias, F. W. C., da Cruz Payão Filho, J., & Moraes e Oliveira, V. H. P. (2021). Prediction of the interpass temperature of a wire arc additive manufactured wall: FEM simulations and artificial neural network. Additive Manufacturing, 48, 102387. https://doi.org/10.1016/j.addma.2021.102387

[15] Zani, M., Panettieri, E., & Montemurro, M. (2024). A metamodel of the wire arc additive manufacturing process based on basis spline entities. Engineering with Computers. https://doi.org/10.1007/s00366-023-01926-4
[16] Béraud, N., Ledoux, Y., Mechekour, E.-H., Vignat, F., & Pourroy, F. (2024). Fast thermal simulation of WAAM processing: Toward manufacturing strategy evaluation. CIRP Journal of Manufacturing Science and Technology, 55, 234-246. https://doi.org/10.1016/j.cirpj.2024.10.007
[17] Rosli, N. A., Alkahari, M. R., Abdollah, M. F. bin, Maidin, S., Ramli, F. R., & Herawan, S. G. (2021). Review on effect of heat input for wire arc additive manufacturing process. *Journal of Materials Research and Technology, 11*, 2127-2145. https://doi.org/10.1016/j.jmrt.2021.02.002
[18] Kim, D. B., Shao, G., & Jo, G. (2022). A digital twin implementation architecture for wire + arc additive manufacturing based on ISO 23247. Manufacturing Letters, 34, 1-5. https://doi.org/10.1016/j.mfglet.2022.08.008
[19] Ben Amor, S., Elloumi, N., Eltaief, A., Louhichi, B., Alrasheedi, N. H., & Seibi, A. (2024). Digital twin implementation in additive manufacturing: A comprehensive review. Processes, 12(6), 1062. https://doi.org/10.3390/pr12061062
[20] Li, H., Shi, X., Wu, B., Raimondi Corradi, D., Pan, Z., & Li, H. (2024). Wire arc additive manufacturing: A review on digital twinning and visualization process. Journal of Manufacturing Processes, 116, 293-305. https://doi.org/10.1016/j.jmapro.2024.03.001
[21] Dellarre, A., Béraud, N., Tardif, N., Vignat, F., Villeneuve, F., & Limousin, M. (2023). Qualify a NIR camera to detect thermal deviation during aluminum WAAM. The International Journal of Advanced Manufacturing Technology, 127(1), 625-634. https://doi.org/10.1007/s00170-023-11587-8
[22] Goldak, J., Chakravarti, A., & Bibby, M. (1984). A new finite element model for welding heat sources. Metallurgical Transactions B, 15(2), 299-305. https://doi.org/10.1007/BF02667333
[23] Fourier, J.-B.-J. (1822). Théorie analytique de la chaleur. Paris: Firmin Didot, père et fils. https://gallica.bnf.fr/ark:/12148/bpt6k1045508v
[24] Chergui, A., Béraud, N., Vignat, F., & Villeneuve, F. (2021). Finite element modeling and validation of metal deposition in wire arc additive manufacturing. In L. Roucoules, M. Paredes, B. Eynard, P. Morer Camo, & C. Rizzi (Eds.), Advances on Mechanics, Design Engineering and Manufacturing III (pp. 61-66). Springer International Publishing. https://doi.org/10.1007/978-3-030-70566-4_11
[25] Dellarre, A., Asservissement thermique du procédé Wire Arc Additive Manufacturing : vers un asservissement des procédés Direct Energy Deposition, Doctoral dissertation, Université Grenoble Alpes, (2024). Thèses.fr. https://theses.fr/2024GRALI111